Inorganic Chemistry

Article

pubs.acs.org/IC

$Na_2EuAs_2S_5$, $NaEuAsS_4$, and $Na_4Eu(AsS_4)_2$: Controlling the Valency of Arsenic in Polysulfide Fluxes

Tarun K. Bera and Mercouri G. Kanatzidis*

Department of Chemistry, Northwestern University, Evanston, Illinois 60208, United States

Supporting Information

ABSTRACT: The reactivity of europium with As species in Lewis basic alkali-metal polysulfide fluxes was investigated along with compound formation and the As^{3+}/As^{5+} interplay vis-à-vis changes in the flux basicity. The compound $Na_2EuAs_2S_5$ containing trivalent As^{3+} is stabilized from an arsenic-rich polysulfide flux. It crystallizes in the monoclinic centrosymmetric space group $P2_1/c$. $Na_2EuAs_2S_5$ has $[As_2S_5]^{4-}$ units, built of corner sharing AsS_3 pyramids, which are coordinated to Eu^{2+} ions to give a two-dimensional (2D) layered structure. A sodium polysulfide flux with comparatively less arsenic led to the As^{5+} containing compounds $NaEuAsS_4$ (orthorhombic, *Ama*2) and $Na_4Eu(AsS_4)_2$ (triclinic, *P*1) depending on Na_2S/S ratio. The $NaEuAsS_4$ and $Na_4Eu(AsS_4)_2$ have a three-dimensional (3D) structure built of $[AsS_4]^{3-}$ tetrahedra coordinated to Eu^{2+} ions. All compounds are semiconductors with optical energy gaps of ∼2 eV.

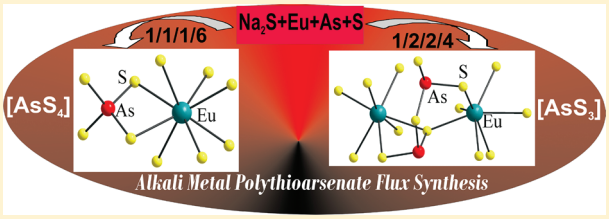

INTRODUCTION

Chalcoarsenate compounds with pyramidal $[AsQ_3]^{3-}$ (Q = S, Se) building units and a stereochemically active lone-pair of electrons on arsenic can have interesting behavior such as glass forming abilities[1] and enhanced nonlinear optical (NLO) second harmonic generation (SHG) properties.[2] The stabilization of As^{3+} species versus As^{5+} is an interesting issue and depends on various factors. For example, the valency of other metal ions present in the system plays an important role, for example, generally higher valent metal ions such as Ta^{5+} or Sn^{4+} favor As^{3+} species, as observed in $KSnAsS_5$, $K_2Sn(AsS_3)_2$, and $K_3Ta_2AsS_{11}$.[3] Conversely, the presence of more Lewis basic low valent metals and cations allows the formation of As^{5+} species. The nature of the synthetic procedures (e.g., alkali-metal polychalcogenide flux[4] versus solvothermal[5]) also plays a role in stabilizing the proper building block anions. Methanothermal reactions have produced a number of As^{3+} containing compounds, for example, $RbAg_2As_3Se_6$, $(Ph_4P)_2(InAs_3S_7)$, $(Me_4N)_2Rb(BiAs_6S_{12})$, among many others.[6] Although the vast majority of thioarsenates involve As^{3+}, this oxidation state is more difficult to stabilize in the oxidizing environment of a polysulfide flux. Since the salt flux can determine the synthetic outcome, we are interested in developing a better understanding of how the two different oxidation states of As are stabilized. In addition, the tendency of As to be oxidized to As^{5+} is greater in a sulfide environment as compared to a selenide environment. This is attributed to the greater electronegativity of sulfur. Here, the polychalcogenide flux synthesis[4] was adopted to synthesize new chalcoarsenates with the oxophilic rare-earths such as Eu. Previously, we reported the synthesis of four As^{3+}-containing Eu-thioarsenates ($AEuAsS_3$; A = Li, K, Rb, and Cs) in an arsenic-rich polysulfide flux.[7] Undoubtedly, the chemistry of arsenic in polychalcogenide fluxes is very different from that of phosphorus.[8] Among known rare earth chalcoarsenates, $Pr_4S_3[AsS_3]_2$,[9] $K_2RE_2As_2Se_9$ (RE = Sm, Gd),[10] $K_3BiAs_6Se_{12}$[11] and $NaCdAsS_3$[12] have been reported. Here we present the synthesis of $Na_2EuAs_2S_5$ (**III**), which features the As^{3+}-containing building unit $[As_2S_5]^{4-}$. From fluxes with a comparatively lower concentration of arsenic, we observed the As^{5+} compounds $NaEuAsS_4$ (**I**) and $Na_4Eu(AsS_4)_2$ (**II**). Fine-tuning of the flux basicity and its role in stabilizing the desired phases is discussed. The thermal and optical behavior of these compounds are correlated with their structures and building units.

EXPERIMENTAL SECTION

Reagents. The chemicals in this work were used as obtained: (i) europium powder, 99.9% purity, <250 μm, Alfa Aesar, Ward Hill, MA; (ii) sulfur powder, sublimed, 99.5%, 100 mesh, Alfa Aesar; (iii) sodium metal cube, 99.95%, Aldrich Chemical Co.; (iv) arsenic, 99.9%, Aldrich Chemical Co.; (v) *N*,*N*-dimethylformamide, Spectrum Chemicals, ACS reagent grade; (vi) diethyl ether, Columbus Chemical Industries, Columbus, WI, ACS reagent grade, anhydrous.

Synthesis of Na_2S. This compound was prepared using a modified literature procedure.[13] In a nitrogen-filled drybox, 9.780 g (0.305 mol) of S was combined with 14.030 g (0.610 mol) of freshly cut sodium metal and placed in a 500-mL round-bottomed flask containing a Teflon-coated stir bar. Liquid ammonia was condensed into the flask at −78 °C (dry ice/acetone bath) under nitrogen until the flask was two-thirds full, resulting in a dark blue/bronze solution. The solution was stirred for ∼5 h and then the ammonia was evaporated as the bath was allowed to warm to room temperature. The light peach solid (∼95% yield, very air sensitive) was dried under vacuum overnight and ground to a fine powder with a mortar and pestle under a dry nitrogen atmosphere in a Vacuum Atmospheres Dry-Lab glovebox.

Received: December 30, 2011
Published: March 13, 2012

   dx.doi.org/10.1021/ic202781c | *Inorg. Chem.* 2012, 51, 4293−4299

Table 1. Crystallographic Refinement Details for $NaEuAsS_4$ and $Na_2EuAs_2S_5$

empirical formula	$NaEuAsS_4$	$Na_2EuAs_2S_5$
formula weight	378.11 g	1016.16 g
temperature	100 K	100 K
wavelength	0.71073 Å	0.71073 Å
crystal system	orthorhombic	monoclinic
space group	*Ama*2	$P2_1/c$
unit cell dimensions	a = 9.9985(18) Å	a = 28.966(2) Å
	α = 90°	α = 90°
	b = 9.9620(17) Å	b = 5.7085(3) Å
	β = 90°	β = 101.270(6)°
	c = 6.7637(12) Å	c = 11.3641(9) Å
	γ = 90°	γ = 90°
volume	673.7(2) Å^3	1842.9(2) Å^3
Z	4	4
density (calculated)	3.728 Mg/m^3	3.663 Mg/m^3
absorption coefficient	15.356 mm^{-1}	15.077 mm^{-1}
θ range for data collection	3.64 to 29.09°	2.87 to 31.88°
reflection collected	3059	20322
independent reflections	953 [R(int) = 0.0644]	6209 [R(int) = 0.0549]
completeness to θ = 31.88°	99.8%	97.9%
refinement method	full-matrix least-squares on F^2	full-matrix least-squares on F^2
data/restraints/parameters	953/1/41	6209/0/190
goodness-of-fit on F^2	1.077	1.219
fnal R indices [$I > 2\sigma(I)^{a,b}$]	R1 = 0.0376	R1 = 0.0484
	wR2 = 0.0637	wR2 = 0.0806
R indices (all data)	R1 = 0.0467	R1 = 0.0648
	wR2 = 0.0661	wR2 = 0.0848
largest diff. peak and hole	1.232 and −1.824 e Å^{-3}	2.056 and −2.667 e Å^{-3}

$^a R1 = \sum||F_o| - |F_c||/\sum|F_o|$. $^b wR2 = \{\sum w(F_o^2 - F_c^2)^2/\sum w(F_o^2)^2\}^{1/2}$.

Synthesis of $NaEuAsS_4$ (I). A mixture of Na_2S (0.059 g, 0.76 mmol), Eu (0.225 g, 1.49 mmol), As (0.111 g, 1.49 mmol), and S (0.167 g, 5.20 mmol) was loaded into a fused silica tube in a nitrogen-filled glovebox. The tube was flame-sealed under vacuum (~10^{-4} mbar) and then heated to 650 °C in 10 h. After 60 h at 650 °C it was cooled to 250 °C in 80 h followed by rapid cooling to room temperature. A dark-red crystalline product in >90% yield (based on Eu) was obtained after carefully breaking the tube. Semiquantitative energy dispersive spectroscopic (EDS) analysis gave an average composition of $Na_{1.1}Eu_{1.0}As_{1.1}S_{4.2}$.

Synthesis of $Na_4Eu(AsS_4)_2$ (II). This compound was isolated from a reaction mixture of Na_2S (0.078 g, 0.99 mmol), Eu (0.150 g, 0.99 mmol), As (0.074 g, 0.99 mmol), and S (0.190 g, 5.93 mmol) using a similar heating profile as above. A red crystalline product was isolated in >70% yield (based on Eu) after removing the excess flux with degassed *N*,*N*-dimethyl formamide (DMF), and EDS gave an average composition of $Na_{4.2}Eu_{1.0}As_{2.1}S_{8.2}$.

Synthesis of $Na_2EuAs_2S_5$ (III). A dark-red crystalline product was isolated in >90% yield (based on Eu) from a reaction mixture of Na_2S (0.046 g, 0.59 mmol), Eu (0.179 g, 1.18 mmol), As (0.088 g, 1.18 mmol), and S (0.076 g, 2.37 mmol) using a similar heating profile as above. Semiquantitative EDS analysis gave an average composition of $Na_{2.1}Eu_{1.0}As_{2.1}S_{5.2}$.

PHYSICAL MEASUREMENTS

Powder X-ray Diffraction Analysis. Powder X-ray diffraction analyses were performed using a calibrated (against NIST silicon) CPS 120 INEL X-ray powder diffractometer (Cu K_α graphite monochromatized radiation) operating at 40 kV/20 mA and equipped with a position-sensitive detector with flat sample geometry. Theoretical powder diffraction patterns from single crystal X-ray data were calculated using the PowderCell, v 2.3 software package.[14]

Table 2. Atomic Coordinates and Equivalent Isotropic Displacement Parameters (Å^2 × 10^3) for $NaEuAsS_4$ and $Na_2EuAs_2S_5$

	x	y	z	U(eq)
		$NaEuAsS_4$		
Na	0.2500	0.3161(7)	0.0933(11)	30(2)
Eu	0.5000	0	0.0378(1)	9(1)
As	0.7500	0.2830(1)	0.0660(3)	6(1)
S(1)	0.5715(2)	0.7871(3)	0.3857(4)	12(1)
S(2)	0.7500	0.9347(3)	0.7950(5)	10(1)
S(3)	0.2500	0.9081(4)	0.2194(5)	7(1)
		$Na_2EuAs_2S_5$		
Na(1)	0.2467(1)	0.7615(6)	0.5530(2)	5(1)
Na(2)	0.2533(1)	0.2590(6)	0.8064(2)	6(1)
Na(3)	0.3428(1)	0.7901(6)	0.8595(3)	11(1)
Na(4)	0.1571(1)	0.2155(6)	0.0158(3)	10(1)
Eu(1A)	0.4533(1)	0.3176(1)	0.9055(1)	4(1)
Eu(1B)	0.4533(3)	0.1790(20)	0.9030(7)	4(1)
Eu(2A)	0.0468(1)	0.6826(1)	0.9520(1)	4(1)
Eu(2B)	0.0466(3)	0.8200(20)	0.9500(7)	4(1)
As(1)	0.5727(1)	0.2435(1)	0.8463(1)	4(1)
As(2)	0.3421(1)	0.2574(1)	0.6204(1)	4(1)
As(3)	0.1582(1)	0.7514(1)	0.7784(1)	4(1)
As(4)	0.9276(1)	0.7598(1)	0.7740(1)	4(1)
S(1)	0.2645(1)	0.2608(3)	0.5604(1)	6(1)
S(2)	0.3505(1)	0.2910(3)	0.8193(1)	7(1)
S(3)	0.6519(1)	0.3505(3)	0.8929(2)	6(1)
S(4)	0.4637(1)	0.4118(3)	0.1775(2)	6(1)
S(5)	0.5571(1)	0.1783(3)	0.0287(2)	7(1)
S(6)	0.9430(1)	0.8214(3)	0.9722(1)	6(1)
S(7)	0.8482(1)	0.6576(3)	0.7413(1)	6(1)
S(8)	0.2359(1)	0.7509(3)	0.7963(1)	6(1)
S(9)	0.0366(1)	0.5867(3)	0.2139(2)	7(1)
S(10)	0.1495(1)	0.7152(3)	0.9688(1)	7(1)

Electron Microscopy. Semiquantitative microprobe analyses of the compounds were performed with a Hitachi S-3400 scanning electron microscope (SEM) equipped with a PGT energy dispersive X-ray analyzer. Data were acquired with an accelerating voltage of 25 kV and a 60s accumulation time.

Solid-State UV/vis/Near-IR Spectroscopy. Optical diffuse reflectance measurements were performed at room temperature using a Shimadzu UV-3101PC double-beam, double-monochromator spectrophotometer. The instrument was equipped with an integrating sphere detector and controlled by a computer. $BaSO_4$ was used as a 100% reflectance standard. The samples were prepared by grinding the crystals to a powder and spreading it on a compacted surface of the powdered standard material, preloaded into a sample holder. The reflectance versus wavelength data generated was used to estimate the band gap of the materials by converting reflectance to absorption data using the Kubelka–Munk equation as discussed previously.[15]

Raman Spectroscopy. Raman spectra were recorded on a BIORAD FT-Raman II spectrograph equipped with a Nd:YAG infrared continuous wave laser (λ = 1064 nm) and a liquid nitrogen cooled germanium detector. A finely powdered sample in a pyrex capillary tube was used for the spectral study after calibrating the spectrometer with KBr. Laser power at the sample was estimated to be about 5 mW, and the focused laser beam diameter was about 10 μm. A total of 20 scans were sufficient to obtain a quality spectrum.

Differential Thermal Analysis (DTA). Thermal analysis was performed on a Shimadzu DTA-50 thermal analyzer. Typically, a sample

dx.doi.org/10.1021/ic202781c | Inorg. Chem. 2012, 51, 4293–4299

Table 3. Anisotropic Displacement Parameters (Å^2 × 10^3) for $NaEuAsS_4$ and $Na_2EuAs_2S_5$

	U^{11}	U^{22}	U^{33}	U^{23}	U^{13}	U^{12}
			$NaEuAsS_4$			
Na	65(5)	12(3)	13(4)	0(3)	0	0
Eu	7(1)	8(1)	13(1)	0	0	−2(1)
As	6(1)	5(1)	6(1)	−2(1)	0	0
S(1)	8(1)	13(1)	14(1)	4(1)	−4(1)	−1(1)
S(2)	10(2)	7(2)	13(2)	−1(2)	0	0
S(3)	7(2)	5(2)	9(2)	1(1)	0	0
			$Na_2EuAs_2S_5$			
Na(1)	7(1)	6(1)	4(1)	0(1)	1(1)	0(1)
Na(2)	5(1)	7(1)	6(1)	2(1)	2(1)	2(1)
Na(3)	10(1)	13(2)	9(1)	5(1)	2(1)	0(1)
Na(4)	10(1)	12(2)	8(1)	−4(1)	2(1)	1(1)
Eu(1A)	5(1)	4(1)	4(1)	−1(1)	1(1)	0(1)
Eu(1B)	5(1)	4(1)	4(1)	−1(1)	1(1)	0(1)
Eu(2A)	5(1)	4(1)	4(1)	0(1)	1(1)	0(1)
Eu(2B)	5(1)	4(1)	4(1)	0(1)	1(1)	0(1)
As(1)	4(1)	4(1)	4(1)	−1(1)	1(1)	0(1)
As(2)	4(1)	5(1)	4(1)	0(1)	1(1)	0(1)
As(3)	4(1)	4(1)	4(1)	−1(1)	1(1)	−1(1)
As(4)	4(1)	4(1)	4(1)	1(1)	0(1)	0(1)
S(1)	6(1)	6(1)	6(1)	1(1)	0(1)	1(1)
S(2)	5(1)	11(1)	4(1)	0(1)	0(1)	0(1)
S(3)	5(1)	6(1)	7(1)	1(1)	1(1)	0(1)
S(4)	6(1)	6(1)	7(1)	1(1)	2(1)	1(1)
S(5)	6(1)	7(1)	6(1)	2(1)	2(1)	1(1)
S(6)	7(1)	7(1)	5(1)	−1(1)	1(1)	0(1)
S(7)	5(1)	6(1)	5(1)	0(1)	0(1)	0(1)
S(8)	5(1)	6(1)	7(1)	1(1)	2(1)	1(1)
S(9)	7(1)	7(1)	6(1)	−1(1)	0(1)	1(1)
S(10)	6(1)	10)6(1)	4(1)	1(1)	2(1)	0(1)

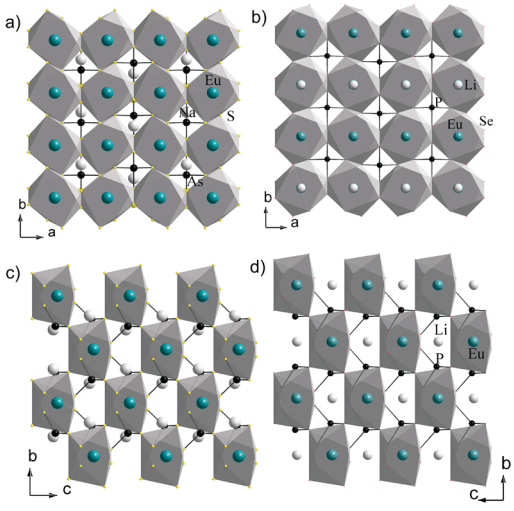

Figure 1. (a) Unit cell view of $NaEuAsS_4$ (**I**) down the *c*-axis shows the edge sharing of EuS_8 polyhedra. (b) Unit cell view of $LiEuPSe_4$ down the *c*-axis. (c) View down the *a*-axis of **I** shows the tunnels formed through the corner sharing of EuS_8 polyhedra and the positions of Na to the side of the tunnel. (d) View down the *a*-axis of $LiEuPSe_4$,[18] showing the position of Li ions in the middle of the tunnels.

(~30 mg) of ground crystalline material was sealed in a silica ampule under vacuum. A similar ampule of equal mass filled with Al_2O_3 was sealed and placed on the reference side of the detector. The sample was heated to 600 at 10 °C/min, and after 1 min, was cooled at a rate of 10 °C/min to 50 °C. The residues of the DTA experiments were examined by X-ray powder diffraction. Reproducibility of the results was confirmed by running multiple heating/cooling cycles. The melting and crystallization points were measured at the minimum of the endothermic peak and at the maximum of the exothermic peak, respectively.

Single-Crystal X-ray Crystallography for $NaEuAsS_4$(I). A dark-red needle was chosen for the single crystal X-ray diffraction study. Data collection was done at 100 K using a STOE imaging-plate diffraction system (IPDS-2)[16] with graphite-monochromatized Mo$K\alpha$ radiation. An analytical absorption correction was applied using the X-area suite program. The shape of the crystal was optimized as a needle using X-Shape. Face indexed data was used to optimize the shape of crystal. Intensity statistics and systematic absences confirm the noncentrosymmetric space group *Ama*2. Direct methods and full-matrix least-squares refinement against F^2 for 41 variables was performed with the SHELXTL package.[17] All 6 atoms were found by running a few cycles of refinement. The structures were inverted by the "MOVE 1 1 1 −1" command at the final stage of refinements. The crystallographic refinement details, fractional atomic coordinates, and anisotropic thermal parameters are shown in Table 1−3.

Single-Crystal X-ray Crystallography for $Na_4Eu(AsS_4)_2$(II). A red needle was chosen for the single crystal X-ray diffraction study. Data collection, data integration, and absorption correction were carried out as above. Direct methods and full-matrix least-squares refinement were performed with the SHELXTL package.[15] A reasonable solution was obtained with triclinic *P*1 symmetry. PLATON suggested additional symmetry, but increasing the crystallographic symmetry did not help to obtain any reasonable solution. The structure is only poorly refined with triclinic *P*1. A rotational twin (−1 0 0, 0 0 1, 0 1 0) fraction was found to be ~3.0% and racemic twin fraction was ~47.9%. Refinement details: *P*1, $Z = 2$, $a = 6.9377(14)$ Å, $b = 9.918(2)$ Å, $c = 9.918(2)$ Å, $\alpha = 90.31(3)$, $\beta = 90.00(3)°$, $\gamma = 90.00(3)°$, $V = 682.5(2)$

dx.doi.org/10.1021/ic202781c | Inorg. Chem. 2012, 51, 4293−4299

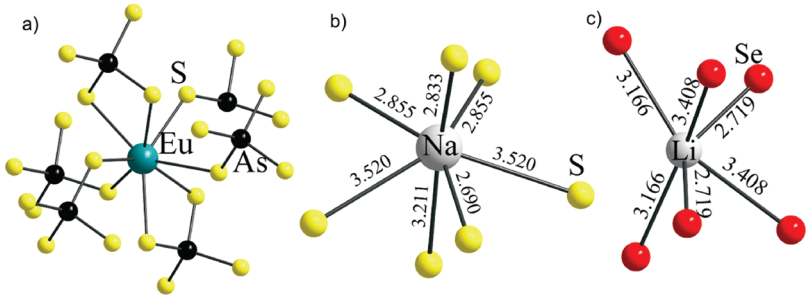

Figure 2. Local coordination environment of (a) Eu and (b) Na in $NaEuAsS_4$. (c) Local coordination environment of Li in $LiEuPSe_4$.[18].

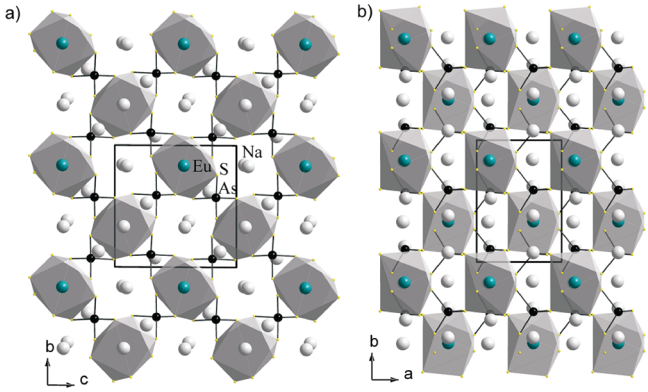

Figure 3. (a) Unit cell view of $Na_4Eu(AsS_4)_2$ (**II**) down the *a*-axis, showing the connectivity of EuS_8 polyhedron through $[AsS_4]^{3-}$. (b) View down the *c*-axis of **II**, showing the tunnel down the *c*-axis.

Å^3, θ_{max} (Mo K_α) = 29.21°, total reflections = 6133, unique reflections $F_o^2 > 2\sigma(F_o^2)$ = 5326, number of variables = 125, μ = 10.714 mm^{-1}, D_c = 3.164 g/cm^3, R_{int} = 4.85%, GOF = 2.087, R_1 = 8.58%.

Single-Crystal X-ray Crystallography for $Na_2EuAs_2S_5$(III). A well-formed dark-red needle was chosen for the single crystal X-ray diffraction study. Data collection, data integration, and absorption correction were similar to those above. Intensity statistics and systematic absences confirm the centrosymmetric space group $P2_1/c$. The structure was solved with direct methods, and full-matrix least-squares refinement against F^2 for 190 variables was performed with the SHELXTL package.[15] All 20-atoms were found by running a few cycles of refinement. After anisotropic refinement of all atoms, R1 was 5.77% but

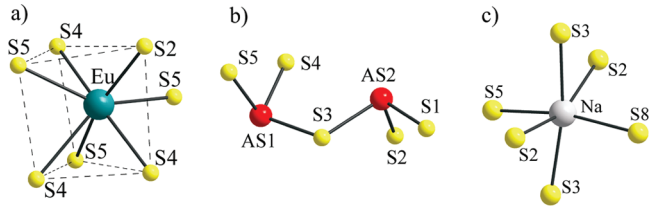

Figure 5. Local coordination environment of (a) Eu, (b) As, and (c) Na atoms in $Na_2EuAs_2S_5$.

there were two residual electron density peaks, ~0.80 Å away from the two europium atoms (Eu1 and Eu2). As a result, a disordered model with split Eu sites was used (Eu1A − Eu1B and Eu2A − Eu2B). The occupancies of Eu1B and Eu2B sites were freely refined to ~4%. The thermal parameters of split sites Eu1A and Eu1B were constrained to be equal by using the EADP command. Final R1 was 4.84%. The crystallographic refinement details, fractional atomic coordinates, and anisotropic thermal parameters are shown in Table 1−3.

RESULTS AND DISCUSSION

Alkali-Metal Polysulfide Flux Synthesis. The synthesis of the dark red As^{5+} compounds $NaEuAsS_4$ (**I**) and $Na_4Eu(AsS_4)_2$ (**II**) was achieved by heating a polysulfide flux mixture of Na_2S/Eu/As/S at 650 °C. An optimum ratio of 0.5/1/1/3.5 led to compound **I**, whereas a more basic flux ratio of 1/1/1/6 yielded compound **II**. The synthesis of $Na_2EuAs_2S_5$ (**III**), which is an As^{3+} compound, was achieved by heating an arsenic-rich flux ratio of 1/2/2/4 (Na_2S/Eu/As/S) at 650 °C. An attempt to stabilize the single $[AsS_3]^{3-}$ units, as in $LiEuAsS_3$,[7] by slightly

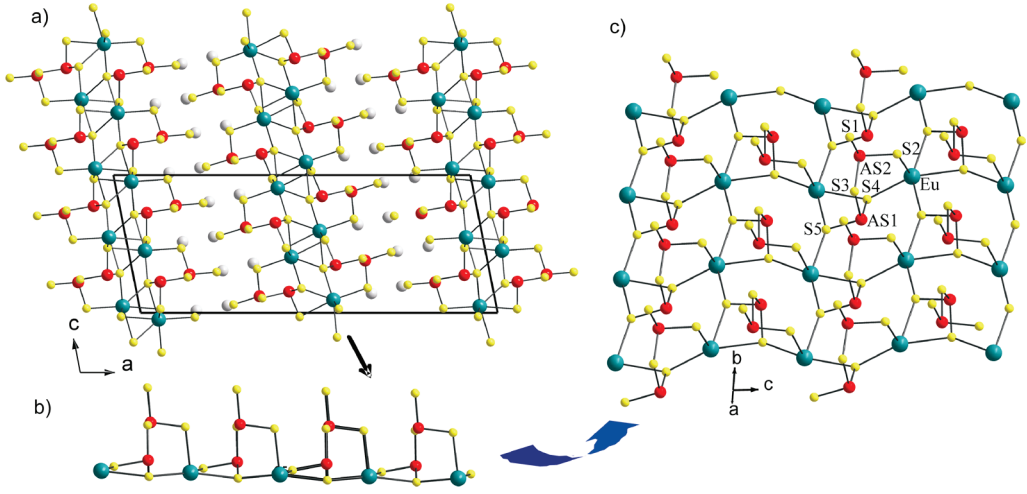

Figure 4. (a) Unit cell view of $Na_2EuAs_2S_5$ (**III**) down the *b*-axis, shows the packing of $^2/_\infty[Eu_2(As_2S_5)_2]^{4-}$ slab with the Na-atoms. View of a single $[EuAs_2S_5]^{2-}$ sublayer down the *b*-axis (b) and the *a*-axis (c). Red atoms are As, yellow atoms are S, light gray atoms are Na.

dx.doi.org/10.1021/ic202781c | Inorg. Chem. 2012, 51, 4293−4299

lowering the arsenic content was unsuccessful and instead gave a mixture of **I** and **II**. These results suggest that a less basic, As-rich flux favors As^{3+} species. The experimental powder X-ray diffraction patterns of all reported compounds matched well with the simulated patterns obtained from the single crystal refinement data (see Supporting Information). However, the powder patterns indicated the presence of Eu_2O_2S[18] as a very minor phase. These compounds are air and moisture sensitive and decompose in open atmosphere in less than 15 min.

Crystal Structures of $NaEuAsS_4$ (I) and $Na_4Eu(AsS_4)_2$ (II). The polar orthorhombic structure of **I** was confirmed by the single crystal X-ray diffraction analysis. It has a polar $^3/_\infty[EuAsS_4^-]$ three-dimensional (3D) network built of $[AsS_4]^{3-}$ tetrahedra connected to Eu atoms, Figure 1a. The $^3/_\infty[EuAsS_4^-]$ framework in $NaEuAsS_4$ is closely related to that of $LiEuPSe_4$ (orthorhombic *Ama*2), Figure 1b,[19] but the difference lies in the arrangement of the alkali-metal sites in the two compounds. A polyhedral representation of the structures of $NaEuAsS_4$ and $LiEuPSe_4$ is shown in Figures 1a, 1c and Figures 1b, 1d, respectively. The $^3/_\infty[EuPnQ_4^-]$ (*Pn* = As, P; Q = S, Se) framework in $NaEuAsS_4$ and $LiEuPSe_4$ has small tunnels down the *a*-axis, Figure 1c, 1d. In the case of $LiEuPSe_4$, the Li atoms reside in the middle of the tunnel, whereas in the structure of $NaEuAsS_4$ the Na atom moves to the side of the tunnel, Figure 1c, 1d. The immediate coordination environment of Na and Li ions is shown in Figure 2b, 2c.

The Eu^{2+} centers are bonded to eight S atoms to form distorted square antiprisms. The Eu^{2+} atoms are surrounded by six $[AsS_4]^{3-}$ tetrahedra, two of which share edges while the remaining four share corners, Figure 2a. The EuS_8 square antiprisms alone form a 3D network by sharing corners in the *bc* plane, edges in the *ab* plane, and corners and edges in the *ac* plane, Figure 1a, 1c.

The above-mentioned positional flexibility of alkali-metals within the $^3/_\infty[EuPnQ_4^-]$ framework is also manifested in the structure of $Na_4Eu(AsS_4)_2$ (**II**), where Na atoms are situated in both the middle and the side of the tunnel to accommodate the increased fraction of Na in the compound compared to $NaEuAsS_4$, Figure 3b. A closer look into the structure confirms that unlike $NaEuAsS_4$ (Figure 1a), the extended 3D network of EuS_8 polyhedra does not exist in $Na_4Eu(AsS_4)_2$ (**II**). The substitution of two Na atoms at every other Eu site in the structure of $NaEuAsS_4$ (Figure 1a) results in the structure of $Na_4Eu(AsS_4)_2$ (**II**), Figure 3a. The As−S bond distances in both **I** and **II** are normal and similar to previously reported compounds.[20]

It is interesting that the alkali-metal-rich phase $Na_4Eu(AsS_4)_2$ actually possesses a 3D framework of $[Eu(AsS_4)_2]$. Generally, alkali-metal-rich phases feature lower dimensionality frameworks relative to that of the alkali-poor counterparts, for example, $AEuPS_4$ vs $A_4Eu(PS_4)_2$ (A = K, Rb, Cs), which have two-dimensional (2D) and one-dimensional (1D) structures, respectively.[8,21,22] The main driving force behind the preservation of a 3D framework in $Na_4Eu(AsS_4)_2$ may be the small size of the cationic volume (due to small Na-ions) compared to the fraction of the anionic volume. Also, the high electropositivity of Na compared to that for the larger alkali-metals K, Rb, or Cs results in stronger interaction with the framework.

Crystal Structure of $Na_2EuAs_2S_5$ (III). Compound **III** crystallizes in the monoclinic centrosymmetric space group $P2_1/c$. It features layers of $^2/_\infty[Eu_2(As_2S_5)_2]^{4-}$ (in the *bc*-plane) that stack along the *a*-axis, Figure 4a. These slabs are separated by layers of Na^+ ions. Each layer of $^2/_\infty[Eu_2(As_2S_5)_2]^{4-}$ is constructed by stitching two $[EuAs_2S_5]^{2-}$ sublayers together through Eu−S bonds, Figure 4b. Unfavorable Eu−Eu interactions between two $[EuAs_2S_5]^{2-}$ sublayers within the slab are avoided by shifting one sublayer relative to the other by ∼1.5 Å along the *c*-axis. The face sharing of EuS_7 polyhedra across the two $[EuAs_2S_5]^{2-}$ sublayers creates a single $^2/_\infty[Eu_2(As_2S_5)_2]^{4-}$ slab. The Eu−Eu distances are 3.743(1) Å, similar to those in $LiEuAsS_3$. In the $[EuAs_2S_5]^{2-}$ sublayer the connectivity between $[As_2S_5]^{4-}$ fragments and the Eu^{2+} ions is unique. It generates a 2D array of Eu-atoms (along the *b*- and *c*-directions) on one side of the layer and $[As_2S_5]^{4-}$ units on the other, Figure 4c.

The coordination environment of Eu^{2+} is distorted monocapped trigonal prismatic with all seven Eu−S distances ranging from 2.929(2)−3.139(2) Å, see Figure 5a and Table 4.

Table 4. Selected Bond Distances in $NaEuAsS_4$ and $Na_2EuAs_2S_5$

$NaEuAsS_4$		$Na_2EuAs_2S_5$		$Na_2EuAs_2S_5$	
Eu−S(3)	2.9317(19)	Eu(1A)−S(2)	2.9496(16)	Na(1)−S(10)	2.792(3)
Eu−S(3)	2.9317(19)	Eu(1A)−S(5)	2.9584(19)	Na(1)−S(8)	2.843(3)
Eu−S(2)	3.061(2)	Eu(1A)−S(4)	2.9708(17)	Na(1)−S(8)	2.873(3)
Eu−S(2)	3.061(2)	Eu(1A)−S(5)	3.003(2)	Na(1)−S(1)	2.895(4)
Eu−S(1)	3.122(3)	Eu(1A)−S(4)	3.0936(17)	Na(1)−S(1)	2.903(4)
Eu−S(1)	3.122(3)	Eu(1A)−S(4)	3.1545(17)	Na(1)−S(3)	2.925(3)
Eu−S(1)	3.247(2)	Eu(1A)−S(5)	3.1617(16)	Na(2)−S(2)	2.796(3)
Eu−S(1)	3.247(2)	Eu(2A)−S(10)	2.9500(16)	Na(2)−S(1)	2.844(3)
As−S(1)	2.162(2)	Eu(2A)−S(6)	2.9576(19)	Na(2)−S(8)	2.851(4)
As−S(1)	2.162(2)	Eu(2A)−S(9)	2.9718(17)	Na(2)−S(1)	2.876(3)
As−S(2)	2.164(4)	Eu(2A)−S(6)	3.001(2)	Na(2)−S(8)	2.942(4)
As−S(3)	2.169(4)	Eu(2A)−S(6)	3.1612(16)	Na(2)−S(7)	2.943(3)
Na−S(3)	2.690(8)	Eu(2A)−S(9)	3.0965(17)	Na(3)−S(2)	2.901(4)
Na−S(2)	2.833(7)	Eu(2A)−S(9)	3.1578(17)	Na(3)−S(3)	2.901(3)
Na−S(1)	2.855(6)	As(1)−S(4)	2.2237(19)	Na(3)−S(2)	2.911(4)
Na−S(1)	2.855(6)	As(1)−S(5)	2.2375(17)	Na(3)−S(3)	2.922(3)
		As(1)−S(3)	2.3337(17)	Na(3)−S(5)	2.934(3)
		As(2)−S(1)	2.2184(17)	Na(3)−S(8)	3.047(3)
		As(2)−S(2)	2.2336(17)	Na(4)−S(7)	2.887(3)
		As(2)−S(3)	2.3363(19)	Na(4)−S(10)	2.902(4)
		As(3)−S(8)	2.2193(17)	Na(4)−S(10)	2.906(4)
		As(3)−S(10)	2.2363(17)	Na(4)−S(7)	2.914(3)
		As(3)−S(7)	2.333(2)	Na(4)−S(6)	2.937(3)
		As(4)−S(9)	2.2251(19)	Na(4)−S(1)	3.054(3)
		As(4)−S(6)	2.2365(17)		
		As(4)−S(7)	2.3295(17)		

dx.doi.org/10.1021/ic202781c | *Inorg. Chem.* 2012, 51, 4293−4299

These are comparable to previously reported europium sulfide compounds.[8b,23] Four out of five S atoms in the $[As_2S_5]^{4-}$ unit are involved in coordination with Eu atoms. The remaining S atom (S1) extended out of the layer to interact solely with Na^+ cations, Figure 5c. The $[As_2S_5]^{4-}$ fragment is constructed from the corner-sharing of two AsS_3 units through S3, Figure 5b. All As−S bond distances are in the range of 2.218(2)−2.236(2) Å and are close to those found in other $[As_2S_5]^{4-}$ containing compounds: $Tl_2MnAs_2S_5$,[24] *hatchite* mineral $TlAgPbAs_2S_5$,[25] $(Me_4N)_2Mo_2O_2As_2S_7$,[26] and thioarsenates with transition metal complex cations.[27] The Na-atoms have a distorted octahedral environment of S atoms, Figure 5c.

Raman Spectroscopy and Optical Absorption. The Raman spectra obtained on polycrystalline samples of **the three compounds** are shown in Figure 6a. The high energy peaks in

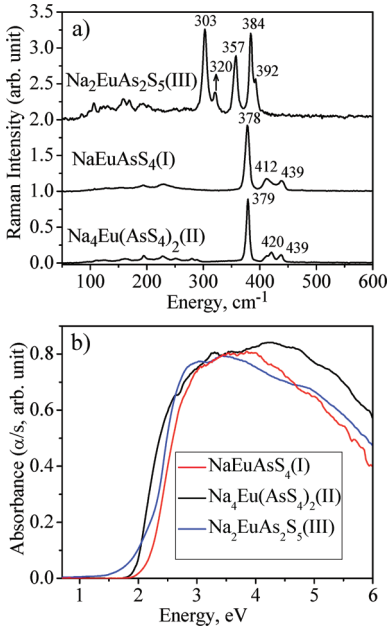

Figure 6. (a) Raman spectra of **I**, **II**, and **III**. (b) Solid-state UV−vis optical absorption spectra for **I**, **II**, and **III**.

the range of 300−440 cm^{-1} are assigned to As−S stretching modes and the low energy peaks in the range of 100−200 cm^{-1} correspond to S−As−S bending modes.[20a] The As−S stretching modes for $Na_2EuAs_2S_5$ are shifted to lower frequencies compared to $NaEuAsS_4$ and $Na_4Eu(AsS_4)_2$ because of the stronger As^{5+}-S bonding in $[AsS_4]^{3-}$ relative to As^{3+}-S bonding in $[As_2S_5]^{4-}$. A similar shift of the As−S stretching modes was observed when comparing $AEuAsS_3$ to $AEuAsS_4$ (A = K, Rb, and Cs).[7] The As−S stretching frequencies in $Na_2EuAs_2S_5$ are spread over a wider range (303−392 cm^{-1}) relative to those of $AEuAsS_3$. This can be accounted for by the increased number of As−S distances and S−As−S angles in the $[As_2S_5]^{4-}$ unit vis-a-vis the $[AsS_3]^{3-}$ unit.

Electronic absorption spectroscopy of ground solid samples showed sharp absorption edges at ∼2.00 eV for all three compounds, consistent with their dark-red color, Figure 6b. The increased fraction of alkali-metals in $Na_4Eu(AsS_4)_2$ (relative to $NaEuAsS_4$) has a negligible effect on the band gap. Similarly, the variation of the thioarsenate building units ($[AsS_4]^{3-}$ versus $[As_2S_5]^{4-}$) does not affect the band gap considerably. This suggests that the optical excitation process is local and originates from occupied S-based p-orbitals dominating the valence band to vacant Eu-based orbitals in the conduction band.

Differential Thermal Analysis. Differential thermal analysis shows a single melting and crystallization event through the entire heating−cooling process for all three compounds, Figure 7a−c. Identical powder diffraction patterns

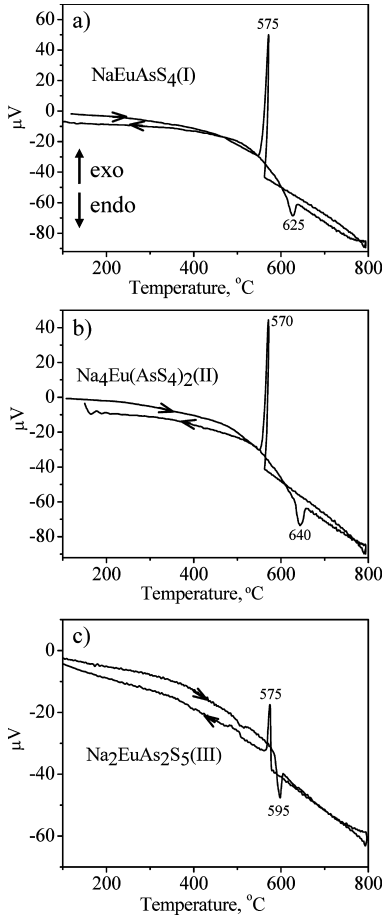

Figure 7. DTA plots of (a) $NaEuAsS_4$, (b) $Na_4Eu(AsS_4)_2$, and (c) $Na_2EuAs_2S_5$.

before and after the DTA confirms the congruent melting behavior. The melting points lie within the temperature range of 575−640 °C and crystallization points in the range of 570−625 °C. Because of the very high melting temperature of Eu_2O_2S (2177 °C),[28] signs of this impurity phase were not detected in the DTA of these compounds.

CONCLUSION

Three new compounds $NaEuAsS_4$, $Na_4Eu(AsS_4)_2$, and $Na_2EuAs_2S_5$ were synthesized in alkali-metal polysulfide fluxes. An arsenic-rich, low basicity flux was found to favor the lower valent As^{3+} in $Na_2EuAs_2S_5$, which otherwise (i.e., arsenic-poor and higher basicity) leads to the As^{5+}-containing phases $NaEuAsS_4$ and $Na_4Eu(AsS_4)_2$. The positional flexibility of the alkali-metals within the polar 3D framework of $^3/_\infty[EuAsS_4^-]$, which results in the two compounds $NaEuAsS_4$ and $Na_4Eu(AsS_4)_2$ with different alkali-metal content and points to the robustness of the framework. This suggests that additional phases with varying alkali-metal content can be stabilized in the A-M-*Pn*-Q (A = Li, Na; M = Eu, Ca, Yb, Sn, and Pb) system

dx.doi.org/10.1021/ic202781c | *Inorg. Chem.* 2012, 51, 4293−4299

with a rich interplay of As^{3+}/As^{5+} chemistry, the details of which is dictated by the nature of M and the basicity of the flux.

■ ASSOCIATED CONTENT

Supporting Information

The powder X-ray patterns, experimental details, and X-ray crystallographic files (CIF) for $NaEuAsS_4$ and $Na_2EuAs_2S_5$. This material is available free of charge via the Internet at http://pubs.acs.org.

■ AUTHOR INFORMATION

Corresponding Author

*E-mail: m-kanatzidis@northwestern.edu.

Notes

The authors declare no competing financial interest.

■ ACKNOWLEDGMENTS

Financial support from the National Science Foundation (Grant DMR-1104965) is gratefully acknowledged. This work made use of the SEM facilities at the Electron Probe Instrumentation Center (EPIC), Northwestern University. FT-Raman spectroscopic study was done at the Analytical Service Laboratory (ASL), Northwestern University.

■ REFERENCES

(1) (a) Zakery, A.; Elliott, S. R. *J. Non-Cryst. Solids* **2003**, *330*, 1. (b) Liang, Z. *J. Non-Cryst. Solids* **1991**, *127*, 298.

(2) (a) Ye, N.; Chen, Q.; Wu, B.; Chen, C. *J. Appl. Phys.* **1998**, *84*, 555. (b) Distanov, V. E. N.; B., G.; Kirdyashkin, A. G.; Serboulenko, M. G. *J. Cryst. Growth* **2002**, *235*, 457. (c) Feichtner, J. D.; Roland, G. W. *Appl. Opt.* **1972**, *11*, 993. (d) Bera, T. K.; Song, J. H.; Freeman, A. J.; Jang, J. I.; Ketterson, J. B.; Kanatzidis, M. G. *Angew. Chem., Int. Ed.* **2008**, *47*, 7828. (e) Bera, T. K.; Jang, J. I.; Ketterson, J. B.; Kanatzidis, M. G. *J. Am. Chem. Soc.* **2009**, *131*, 75. (f) Song, J. H.; Freeman, A. J.; Bera, T. K.; Chung, I.; Kanatzidis, M. G. *Phys. Rev. B* **2009**, *79*, 245203. (g) Bera, T. K.; Song, J. H.; Freeman, A. J.; Jang, J. I.; Ketterson, J. B.; Kanatzidis, M. G. *J. Am. Chem. Soc.* **2010**, *132*, 3484.

(3) (a) Iyer, R. G.; Do, J.; Kanatzidis, M. G. *Inorg. Chem.* **2003**, *42*, 1475. (b) Iyer, R. G.; Kanatzidis, M. G. *Inorg. Chem.* **2002**, *41*, 3605. (c) Iyer, R. G.; Bilc, D.; Mahanti, S. D.; Kanatzidis, M. G. *Solid-State Chem. Inorg. Mater.* **2005**, *848*, 83. (d) Do, J.; Kanatzidis, M. G. *J. Alloys Compd.* **2004**, *381*, 41.

(4) (a) Kanatzidis, M. G.; Sutorik, A. C. *Prog. Inorg. Chem.* **1995**, *43*, 151. (b) Sunshine, S. A.; Kang, D.; Ibers, J. A. *J. Am. Chem. Soc.* **1987**, *109*, 6202. (c) Kanatzidis, M. G.; Park, Y. *Chem. Mater.* **1990**, *2*, 99.

(5) Sheldrick, W. S.; Wachhold, M. *Angew. Chem., Int. Ed. Engl.* **1997**, *36*, 206.

(6) (a) Pan, Y.; Jin, Q.; Chen, J.; Zhang, Y.; Jia, D. *Inorg. Chem.* **2009**, *48*, 5412. (b) Wang, X.; Sheng, T.-L.; Hu, S.-M.; Fu, R.-B.; Chen, J.-S.; Wu, X.-T. *J. Solid State Chem.* **2009**, *182*, 913. (c) Wachhold, M.; Kanatzidis, M. G. *Inorg. Chem.* **2000**, *39*, 2337. (d) Wachhold, M.; Kanatzidis, M. G. *Inorg. Chem.* **1999**, *38*, 3863. (e) Wachhold, M.; Kanatzidis, M. G. *Z. Anorg. Allg. Chem.* **2000**, *626*, 1901. (f) Chou, J.-H.; Kanatzidis, M. G. *Inorg. Chem.* **1994**, *33*, 1001. (g) Fu, M.-L.; Guo, G.-C.; Liu, X.; Chen, W.-T.; Liu, B.; Huang, J.-S. *Inorg. Chem.* **2006**, *45*, 5793. (h) Dehnen, S.; Melullis, M. *Coord. Chem. Rev.* **2007**, *251*, 1259. (i) Chou, J. H.; Hanko, J. A.; Kanatzidis, M. G. *Inorg. Chem.* **1997**, *35*, 4.

(7) Bera, T. K.; Kanatzidis, M. G. *Inorg. Chem.* **2008**, *47*, 7068.

(8) (a) Evenson, C. R.; Dorhout, P. K. *Inorg. Chem.* **2001**, *40*, 2875. (b) Evenson, C. R.; Dorhout, P. K. *Inorg. Chem.* **2001**, *40*, 2884. (c) Aitken, J. A.; Chondroudis, K.; Young, V. G. Jr.; Kanatzidis, M. G. *Inorg. Chem.* **2000**, *39*, 1525. (d) Kanatzidis, M. G. *Curr. Opin. Solid State Mater. Sci.* **1997**, *2*, 139.

(9) Kang, D.; Schleid, T. *Z. Anorg. Allg. Chem.* **2009**, *635*, 2170.

(10) Wu, Y. D.; Bensch, W. *Inorg. Chem.* **2009**, *48*, 2729.

(11) Wu, Y. D.; Bensch, W. *J. Alloys Compd.* **2011**, *509*, 4452.

(12) Wu, Y. D.; Bensch, W. *J. Alloys Compd.* **2012**, *511*, 35.

(13) Feher, F. *Handbuch der Präparativen Anorganischen Chemie*; Brauer, G., Ed.; Ferdinand Enke: Stuttgart, Germany, 1954; Vol. *1*, pp 280−281.

(14) Kraus, W.; Nolze, G. *PowderCell* 2.3; Federal Institute for Materials Research and Testing (BAM) : Berlin, Germany, 1998.

(15) (a) Pankove, J. I. In *Optical Processes in Semiconductors*; Dover Publications: New York, 1975. (b) Kanatzidis, M. G.; McCarthy, T. J.; Tanzer, T. A.; Chen, L. H.; Iordanidis, L.; Hogan, T.; Kannewurf, C. R.; Uher, C.; Chen, B. X. *Chem. Mater.* **1996**, *8*, 1465. (c) Liao, J. H.; Kanatzidis, M. G. *Chem. Mater.* **1993**, *5*, 1561. (d) Trikalitis, P. N.; Rangan, K. K.; Bakas, T.; Kanatzidis, M. G. *J. Am. Chem. Soc.* **2002**, *124*, 12255.

(16) *X-Area*, Version 1.39; STOE & Cie GmbH: Darmstadt, Germany, 2006.

(17) *SHELXTL*, Version 5.03; Siemens Analytical X-ray Instruments: Madison, WI, 1995.

(18) Eick, H. A. *J. Am. Chem. Soc.* **1958**, *80*, 43. Bakhtiyarov, I. B.; Rustamov, P. G.; Nakhmetov, S. M.; Gasymov, V. A. *Z. Anorg. Allg. Chem.* **1986**, *533*, 186.

(19) Aitken, J. A.; Chondroudis, K.; Young, V. G.; Kanatzidis, M. G. *Inorg. Chem.* **2000**, *39*, 1525.

(20) (a) Wu, Y.; Naether, C.; Bensch, W. *Inorg. Chem.* **2006**, *45*, 8835. (b) Korzenski, M. B.; Schimek, G. L.; Kolis, J. W. *Solid State Sci.* **2000**, *2*, 377. (c) Iyer, R. G.; Kanatzidis, M. G. *Inorg. Chem.* **2004**, *43*, 3656.

(21) Chondroudis, K.; McCarthy, T. J.; Kanatzidis, M. G. *Inorg. Chem.* **1996**, *35*, 840.

(22) (a) Kanatzidis, M. G. *Phosphorus, Sulfur Silicon Relat. Elem.* **1994**, *93*, 159. (b) Sayettat, J.; Bull, L. M.; Gabriel, J. C. P.; Jobic, S.; Camerel, F.; Marie, A. M.; Fourmigue, M.; Batail, P.; Brec, R.; Inglebert, R. L. *Angew. Chem., Int. Ed.* **1998**, *37*, 1711. (c) Kim, K. W.; Kanatzidis, M. G. *J. Am. Chem. Soc.* **1998**, *120*, 8124.

(23) Aitken, J. A.; Larson, P.; Mahanti, S. D.; Kanatzidis, M. G. *Chem. Mater.* **2001**, *13*, 4714.

(24) Gostojic, M.; Edenharter, A.; Nowacki, W.; Engel, P. *Z. Kristallogr.* **1982**, *158*, 43.

(25) Takéuchi, Y.; Ohmasa, M.; Nowacki, W. *Z. Kristallogr.* **1968**, *127*, 349.

(26) Chou, J.-H.; Hanko, J. A.; Kanatzidis, M. G. *Inorg. Chem.* **1997**, *36*, 4.

(27) (a) Pan, Y.; Jin, Q.; Chen, J.; Zhang, Y.; Jia, D. *Inorg. Chem.* **2009**, *48*, 5412. (b) Jia, D. X.; Zhao, Q. X.; Dai, J.; Zhang, Y.; Zhu, Q. Y., Z. *Anorg. Allg. Chem.* **2006**, *632*, 349. (c) Jia, D. X.; Zhao, Q. X.; Song, L. F.; Zhang, Y.; Dai, C. *Chin. J. Struct. Chem.* **2006**, *25*, 1110. (d) Kromm, A.; Sheldrick, W. S. *Z. Anorg. Allg. Chem.* **2008**, *634*, 121. (e) Kanatzidis, M. G.; Chou, J.-H. *J. Solid State Chem.* **1996**, *127*, 186.

(28) Bakhtiyarov, I. B.; Rustamov, P. G.; Nakhmetov, S. M.; Gasymov, V. A. *Z. Anorg. Allg. Chem.* **1986**, *533*, 186.